Published in final edited form as:
Hum Brain Mapp. 2012 June ; 33(6): 1334–1351. doi:10.1002/hbm.21285.

Spatio-Temporal Brain Mapping of Spatial Attention Effects on Pattern-Reversal ERPs

Francesco Di Russo[1,2], **Alessandra Stella**[1,3], **Grazia Spitoni**[2,3], **Francesca Strappini**[3], **Stefano Sdoia**[1], **Gaspare Galati**[2,3], **Steven A. Hillyard**[4], **Donatella Spinelli**[1,2], and **Sabrina Pitzalis**[1,2]

[1]Dept. of Education Sciences for Motor Activity and Sport, University of Rome "Foro Italico" - Rome, Italy

[2]Neuropsychology Center, Santa Lucia Foundation, IRCCS – Rome, Italy

[3]Dept. of Psychology, University of Rome "La Sapienza" - Rome, Italy

[4]Dept. of Neurosciences, University of California San Diego – La Jolla CA, USA

Abstract

Recordings of event-related potentials (ERPs) were combined with structural and functional magnetic resonance imaging (fMRI) to investigate the timing and localization of stimulus selection processes during visual-spatial attention to pattern-reversing gratings. Pattern reversals were presented in random order to the left and right visual fields at a rapid rate while subjects attended to the reversals in one field at a time. On separate runs stimuli were presented in the upper and lower visual quadrants. The earliest ERP component (C1, peaking at around 80 ms), which inverted in polarity for upper versus lower field stimuli and was localized in or near visual area V1, was not modulated by attention. In the latency range 80-250 ms multiple components were elicited that were increased in amplitude by attention and were co-localized with fMRI activations in specific visual cortical areas. The principal anatomical sources of these attention-sensitive components were localized by fMRI-seeded dipole modeling as follows: P1 (ca. 100 ms--source in motion-sensitive area MT+), C2 (ca. 130 ms-- same source as C1), N1a (ca. 145 ms-- source in horizontal intraparietal sulcus), N1b (ca. 165 ms-- source in fusiform gyrus, area V4/V8), N1c (ca. 180 ms-- source in posterior intraparietal sulcus, area V3A), and P2 (ca. 220 ms-- multiple sources, including parieto-occipital sulcus, area V6). These results support the hypothesis that spatial attention acts to amplify both feed-forward and feedback signals in multiple visual areas of both the dorsal and ventral streams of processing.

Introduction

A basic goal of attention research is to identify the processing stages at which sensory inputs are modulated (enhanced or suppressed) under top-down control. In humans, scalp recordings of event-related potentials (ERPs) to attended and unattended visual stimuli have provided information on the timing of stimulus selection processes in the visual pathways. Studies over the past three decades have shown that early ERP components in the 80-250 ms range are enhanced in amplitude by spatially focused attention in the manner of a sensory gain control (Hillyard et al., 1998; Hillyard & Anllo-Vento 1998; Hopfinger et al. 2004; Hopf et al. 2009). While ERP and magnetoencephalographic (MEG) recordings have defined the time course of attentional selection processes with a high degree of precision (of

Corresponding author: Dr. Francesco Di Russo, University of Rome "Foro Italico", Piazza Lauro De Bosis, 15, 00135 Rome, Italy, Tel: +390636733383 \ Fax: +390636733387, francesco.dirusso@uniroma4.it, URL: http://digilander.libero.it/francesco.di_russo.

the order of ms), the anatomical localization of the underlying neural activity can only be approximated on the basis of surface recordings. In order to improve the accuracy of localizing the neural sources of ERP/MEG components, many recent studies have combined surface recordings with the spatially more precise hemodynamic measures provided by functional magnetic resonance imaging (fMRI) (e.g., Martinez et al., 2001; Dale & Halgren 2001; Murray et al., 2002; Di Russo et al., 2002b, 2005; Vanni et al., 2004; Schoenfeld et al. 2007; Valdes-Sosa et al., 2009). In studies of visual-spatial attention that combined ERP or MEG recordings with fMRI it was found that the earliest evoked component (the C1 at 50-80 ms), which has been attributed to a primary visual cortex (V1) generator, was not affected by attention, but later components were enhanced in multiple areas of extrastriate visual cortex (e.g. Martinez et al., 2001; Noesselt et al., 2002; Di Russo et al., 2003).

Most ERP studies of attention have used briefly flashed pattern-onset stimuli. An equally effective stimulus that has been used extensively for clinical evaluations (Halliday 1992) is the pattern-reversal produced by abruptly interchanging the light and dark elements of a grating or checkerboard. The pattern-reversal stimulus differs importantly from the pattern-onset in being continuously present throughout recording and in producing a clear perception of motion during the reversal. It is typically reported that the pattern-reversal visual evoked potential (VEP) consists of three main components, termed N75, P100 and N145 (e.g. Nakamura et al., 1997; Shigeto et al., 1998, Hashimoto et al., 1999). In a recent study Di Russo and coworkers (2005) combined VEPs with fMRI and brain mapping methods (retinotopy and cortical surface reconstruction) to obtain a comprehensive spatio-temporal picture of the pattern-reversal VEPs and its neural generators. The results provided strong evidence that the N75 component (also called C1) arises from activity in the primary visual cortex (area V1), while several subsequent components could be accounted for by sources that were in close proximity to fMRI activations found in specific cortical areas: P100 in area MT+, N135 (also called C2) in area V1, N150 in parietal areas, N160 in ventral occipital areas, and N180 in dorsal occipital areas. These latter negativities (from 135 to 180 ms) appear to encompass the well-known N145 and are similar to a sequence of negative components (the “N1 complex”) that was observed in the pattern-onset VEP (Di Russo et al. 2002). These results demonstrate that combining VEPs, fMRI and brain mapping methods while using focal stimuli may reveal the spatio-temporal complexity of evoked neural activity patterns in the visual cortex.

Previous studies of spatial attention to pattern-reversal stimuli used rapid, repetitive (steady-state) stimulus presentations (Di Russo & Spinelli 1999a,b, 2002a; Di Russo et al., 2001). The steady-state visual ERP is a sinusoidal oscillatory response that has been shown to provide a sensitive index of the allocation of attention to repetitive stimuli at different locations in the visual field (Muller et al. 1998, 2003). Steady-state ERP amplitudes to pattern reversal stimuli have been investigated as a function of several stimulus parameters that included pattern contrast and chromaticity. Recordings from a mid-occipital sensor showed that spatial attention enhanced steady-state amplitudes for both chromatic and achromatic stimuli but reduced the apparent latencies for achromatic stimuli only (reviewed in Di Russo et al. 2002c). These results are consistent with the hypothesis that attention acts on cortical gain control mechanisms, which are known to be different for the magno- and parvo-cellular systems.

While these steady-state experiments show that pattern-reversal ERPs are affected by spatial attention, the previous use of only a single scalp sensor does not allow inferences to be made about the neural sources of these attentional modulations. Furthermore, the use of full- or half-field visual stimuli as in previous studies does not allow for clear separation of the neural sources. In particular, stimuli that span more than one visual quadrant (crossing the horizontal or vertical meridians) may activate neural populations with opposing geometry

(as in the primary visual area), resulting in cancellation of concurrent electric fields and misinterpretation of the underlying sources (Regan, 1989; Di Russo et al., 2005).

The present study investigated the effect of spatial attention on the transient pattern-reversal ERP using a dense electrode array and focal stimulation in each of the visual quadrants. The aim was to determine the spatio-temporal profile of attention-related ERP modulations and to localize their neural generators. For this purpose we used the same combined ERP/fMRI technique and stimulation paradigm developed by Di Russo and colleagues (2005). Cortical sources were identified using dipole modeling based on a realistic head model, taking into account the loci of cortical activation revealed by fMRI while performing the same task. These sources were also localized on flat maps with respect to visual cortical areas identified in individual subjects by wide field retinotopic mapping (e.g., Sereno et al., 1995; Pitzalis et al., 2006). In addition, two motion-sensitive cortical areas were individually mapped: the classic lateral area MT+ (Tootell et al., 1995), which was previously found to be strongly activated by pattern-reversal stimuli (Di Russo et al., 2005), and a newly defined medial area labeled V6 (e.g. Pitzalis et al., 2006, 2010; Fattori et al., 2009). It was found that spatial attention produced robust modulations of pattern-reversal evoked activity that could be localized to multiple visual areas in the occipital, parietal, and temporal lobes.

Methods

Subjects

Thirty paid volunteer subjects (16 females, mean age of 25.8, range 18-36 years) participated in the main ERP experiment; a subset of 13 of these subjects (8 females, mean age 26.4 range 21-36 years) also received structural MRI and fMRI scanning. All subjects were right-handed and had normal or corrected-to-normal vision. All participants gave written informed consent prior to both electrophysiological and neuroimaging procedures, which were approved by local ethics and human subjects committees. Before scanning, subjects were allowed, if they desired, to consume a single cup of coffee to better maintain alertness during the scan sessions.

ERP Experiment

Stimuli

The standard stimuli (90% of total) consisted of circular Gabor patterns modulated horizontally in black and white, having a diameter of 3° of visual angle, a spatial frequency of 4 cycles per degree and a mean contrast of 32% (Figure 1). Stimulus events were phase reversals (180° shift) for 66 ms followed by return to the original phase (pattern-reversal stimulation). The background luminance (22 cd/m^2) was equiluminant with the mean luminance of the pattern. Stimuli were presented in the superior (upper quadrants) or inferior (lower quadrants) hemifields on separate runs. During each run stimuli were presented to the left or right quadrants in a pseudo-randomized sequence; stimuli were centered along an arc that was equidistant (4°) from the fixation point and located at a polar angle of 25° above (upper quadrants) or 45° below (lower quadrants) the horizontal meridian. The stimuli were presented asymmetrically in this way so that the upper and lower field stimuli would activate approximately opposing sites on the lower and upper banks of the calcarine fissure, respectively, in light of evidence that the horizontal meridian is actually represented on the lower bank rather than in the lateral recess of the calcarine fissure (e.g., Clark et al., 1995;Aine et al., 1996;Di Russo et al., 2002b,2003).

Phase-shifts occurred in random order in the left or right quadrants at a rapid presentation rate, with SOAs varying between 350-650 ms. Target stimuli (10% of total), were phase reversals of the Gabor gratings that were obliquely oriented but otherwise identical to the

standard reversals. Targets rotated from horizontal to oblique during the phase reversal and were pseudo-randomly intermixed with the standards. A cue made up of four small arrows surrounding the fixation cross indicated the visual quadrant to which attention had to be covertly focused.

Procedure

During the ERP recordings subjects were comfortably seated in a dimly lit, sound-attenuated and electrically shielded chamber while viewing stimuli presented on a 24-inch video monitor with a refresh rate of 60 Hz at a distance of 114 cm. Subjects were trained to maintain stable binocular fixation on a central cross (0.2×0.2°) throughout stimulus presentation. Each ERP run lasted for 120 s, followed by a 30 s rest period, with occasional longer breaks interspersed. A total of 20 runs (10 with stimuli in the upper hemifield and 10 in the lower hemifield) were carried out in order to deliver at least 700 standard stimuli to each quadrant. Subjects were instructed to direct their attention covertly (without moving their eyes) to the quadrant indicated by the direction of the spatial cue. On a given run, stimuli were presented only to either the upper or lower hemifields, with the right/left order randomized. The subject's task was to detect and respond to the infrequent targets at the cued location with a button press while ignoring the stimuli in the opposite field. The order of attending to different quadrants was counterbalanced across runs. The responding hand was similarly counterbalanced across runs. Responses were classified as hits if they occurred within a 200-1200 ms window after the target onset and as anticipatory or delayed responses otherwise. Subjects received a preliminary warm-up session in which they were trained to discriminate the target and achieve an average hit rate of 75-80%. The difficulty of the target discrimination, determined by the orientation difference between standards and targets, was adjusted between runs if necessary to maintain this level of performance. The subjects received feedback on their behavioral performance and their ability to maintain fixation as monitored by the electro-oculogram (EOG).

Electrophysiological Recording and Data Analysis

The EEG was acquired using a BrainVision^{tm} system (BrainProducts, Germany), with 64 electrodes placed according to the 10-10 system montage (Di Russo et al., 2002b). All scalp channels were referenced to the left mastoid (M1). Horizontal eye movements were monitored with a bipolar recording from electrodes at the left and right outer canthi. Blinks and vertical eye movements were recorded with an electrode below the left eye, which was referenced to site Fp1. The EEG was digitized at 250 Hz with an amplifier band-pass of 0.1 to 100 Hz including a 50 Hz notch filter and was stored for off-line averaging. Computerized artifact rejection was performed prior to signal averaging in order to discard epochs in which deviations in eye position, blinks, or amplifier blocking occurred. On average, 8% of the trials were rejected for violating artifact criteria.

Time locked ERPs to standard stimuli were averaged separately according to stimulus position (upper left, upper right, lower left, lower right) and whether the position was attended or unattended. The EEG was segmented into 1100 ms epochs that began 100 ms prior the phase-shift to establish a voltage baseline. In order to reduce high-frequency noise, the averaged ERPs were low-pass filtered at 35 Hz. ERPs to standards that were preceded by a target stimulus within 1000 ms or followed by a target within 500 ms were not averaged to avoid any possible contamination by ERPs related to target detection or motor responses. Component latencies and amplitudes were measured as peak voltage deflections within specified time intervals (see Table I); these measures were taken at the electrode sites where the components were maximal in amplitude in the grand averaged waveforms for each quadrant (Table I). One-way ANOVAs were used to evaluate attention effects on each of the prominent ERP components (C1, P1, N1a, N1b, N1c, and P2), comparing attended vs.

unattended conditions for measures of peak amplitude and latency in the four quadrants. The confidence α level was set to 0.05 after Greenhouse-Geisser correction.

Modeling of ERP Sources

Topographical maps of scalp voltage over time were calculated for ERPs to attended and unattended stimuli and for the difference waves obtained subtracting the unattended from the attended ERPs. Estimation of the dipolar sources of the difference wave components in the grand-average waveforms was carried out using Brain Electrical Source Analysis (BESA 2000 v.5.1.8; Megis, Germany). The algorithm implemented in BESA estimates the location and orientation of multiple equivalent dipolar sources by calculating the scalp distribution that would be obtained for a given dipole model (forward solution) and comparing it to the actual ERP distribution. Interactive changes in the location and orientation in the dipole sources lead to minimization of the residual variance (RV) between the model and the observed spatio-temporal ERP distribution. The present analysis used a realistic approximation of the head with the radius obtained from the average of the group of subjects (81 mm). This realistic head model uses finite elements derived from an average of 24 individual MRIs and consists of three compartments: brain (including the cerebral spinal fluid), skull and scalp. A spatial digitizer recorded the three-dimensional coordinates of each electrode and of three fiducial landmarks (the left and right preauricular points and the nasion). A computer algorithm was used to calculate the best-fit sphere that encompassed the array of electrode sites and to determine their spherical coordinates. The mean spherical coordinates for each site averaged across all subjects were used for the topographic mapping and source localization procedures and were related to the corresponding digitized fiducial landmarks and to landmarks identified on the standard finite element model of BESA 2000. The possibility of interacting dipoles was reduced by selecting solutions with relatively low dipole moments with the aid of an “energy” constraint weighted 20% in the compound cost function, as opposed to 80% for the residual variance (for further explanation of this strategy see Di Russo et al. 2002b). The optimal set of parameters was found in an iterative manner by searching for a minimum in the compound cost function.

A mixed fitting/seeding strategy was used to model the dipolar sources of the ERP attention effects: Single sources were first fit over specific latency ranges to correspond with the distinctive components in the waveform, then were constrained (seeded) to the nearest attention-related fMRI activation and were fit again in orientation only. Source modeling followed a sequential approach: dipoles accounting for the earlier portions of the waveform were left in place as additional dipoles were added. Thus, the number of dipoles chosen for these models corresponded to the major topographical features of the ERP waveforms. The rationale of this strategy was to use the anatomically more precise fMRI information to improve the spatio-temporal modeling of the attention-related neural activity.

fMRI Experiments

fMRI Protocols

In the fMRI experiments both block-sequence and phase-encoded experimental designs were used. First, we used a two-condition block sequence paradigm (eight 16 s ON, 16 s OFF epochs) for the Pattern-Reversal Attention experiment and for mapping motion areas MT+ and V6. Then, we used periodic stimuli and phase-encoding to map the retinotopic visual areas. The four specific fMRI protocols were as described below:

Pattern-Reversal Attention Experiment—In this fMRI experiment, the pattern-reversal stimulation (both temporal and spatial parameters) and task were identical to those used in the ERP experiment, except for the number and duration of runs. The fMRI

experiment consisted of eight runs of 4 min each. A two-condition block sequence paradigm was used, where the two conditions consisted of attention to the left or to the right stimulus sequence. During each run, the left and right quadrants were alternately cued for 16 s each (32 s/cycle, eight cycles/scan). Upper and lower quadrants were tested in separate sessions of four runs each. Prior to scanning, each subject was trained on the task outside the scanner until he/she was completely familiar with the task and was able to maintain central fixation consistently. Stimuli were generated by a control computer located outside the MR room running in-house software implemented in MATLAB (The MathWorks Inc., Natick, MA, USA) using Cogent 2000 (developed at FIL and ICN, UCL, London, UK) and Cogent Graphics (developed by John Romaya at the LON, Wellcome Department of Imaging Neuroscience, UCL, London, UK).

MT+ Mapping—Two additional scans were acquired to localize the motion-sensitive region MT+ Stimuli were produced by an X11/OpenGL program (original GL code by A. Dale, ported and extended by M. Sereno) and consisted of concentric thin light gray rings (0.2 cycles/deg, duty cycle = 0.2) on a slightly darker-gray background, either moving (7 deg/s - ON period) or stationary (OFF period). During the ON block, the concentric rings periodically contracted and expanded over a 2 s cycle to avoid generating motion aftereffects during the OFF block. The average background luminance was 61 cd/m^2, and the luminance contrast of the rings was low (~1.5%) to better isolate MT+ (Tootell et al. 1995). It is now generally acknowledged that the relatively large motion-sensitive region found using this localizer and originally labeled V5 (or MT) in humans (e.g. Tootell et al. 1995) is probably a complex of several areas (see also Pitzalis et al., 2010). For this reason, here we refer to this region as the “MT complex” or “MT+.”

V6 Mapping—An additional two scans were acquired in separate sessions to define the medial motion sensitive area V6, as described by Pitzalis and colleagues (2010). The same X11/OpenGL software (Dale and Sereno) produced 16-s blocks of coherent dot field motion contrasted with 16-s blocks of scrambled motion. A new field of white dots was generated every 500 ms (dot size 0.4 × 0.4 deg). These dots immediately began to move along trajectories that defined either coherent motion or random movements. The coherent motion patterns were chosen randomly for each 500 ms period from a continuum ranging from dilation to outward spiral, to rotation, to inward spiral, to contraction. The center of the movement was jittered from flow to flow, and the speed varied within a small range. During the scrambled OFF period, dots and their movement vectors were generated as during the coherent ON periods except that each dot trajectory was rotated by a random angle. This scrambled the coherency of movement (at a given point, dots moved in different directions) but preserved the speed gradient (central dots still moved slower than peripheral dots). The average luminance of the stimulus was 31 cd/m^2.

Retinotopic Mapping—We mapped polar angle (measured from the contralateral horizontal meridian around the center of gaze) and eccentricity (distance from the center-of-gaze) using the same phase-encoded retinotopic stimuli previously used to map the visuotopic organization of human area V6 (Pitzalis et al. 2006). High contrast light and dark colored checks were counterphase flickered in either a ray- or a ring-shaped configuration (polar angle and eccentricity, respectively). The average luminance of the stimuli was 105 cd/m2. Each subject was presented with periodic stimuli (64 s/cycle, 8 cycles/scan), varying in eccentricity or polar angle, in at least two pairs of scans. Stimuli moved slowly and continuously, and checks reversed between bright and dark at a rate of 8 Hz. Subjects viewed polar angle stimuli moving in both clockwise and counterclockwise directions in separate sessions.

Experimental Set-up

Visual stimuli were projected using an LCD video projector with a customized lens to a back projection screen mounted behind the MR tube and visible through a mirror placed inside the head coil. For the attention experiment the average viewing distance was 66.5 cm, and the screen size was 23×12°. For both retinotopic and motion mapping a wide-field screen was used at a viewing distance of 20 cm, and the standard mirror was enlarged so that the most peripheral part of the screen was in view. This setup allowed a field of view that subtended up to 69° horizontally, 55° vertically, and 82° in an oblique direction. Besides better revealing cortical areas that represent the periphery, such wide field retinotopic stimulation also helped to avoid confounds in fMRI mapping due to surround inhibition. As explained previously (e.g. Pitzalis et al. 2006), retinotopic cortical regions having representations of visual space just beyond the peripheral edge of a rotating wedge can generate a periodic signal with a misleading 180° phase offset. By stimulating most of the visual field, such phase inversion is greatly reduced. In all experiments, fixation distance and head alignment were held constant by a chin rest mounted inside the head coil. Subjects' heads were stabilized with foam padding in order to minimize movement during the scans. In the attention experiment, the subject's manual responses were recorded using a magnet-compatible response pad connected to the control computer via optic fibers. Retinotopic and motion mapping experiments used passive viewing and continuous central fixation throughout the period of scan acquisition.

Imaging parameters

The MR experiments were conducted at the Santa Lucia Foundation (Rome, Italy) on a 3T MR scanner (Siemens Allegra, Siemens Medical Systems, Erlangen). Single shot echo-planar imaging (EPI) images were collected using a standard transmit-receive birdcage head coil. The 30 imaged coronal slices were each 2.5 mm thick (with a 0 mm gap, interleaved excitation order), with an in-plane resolution of 3 × 3 mm, oriented approximately perpendicular to the calcarine fissure. This voxel size strikes a compromise between sufficient signal-to-noise and the ability to assign activations to the correct sides of the sulci and gyri. Each scan took either 256 s (two-condition experiments), or 512 s (retinotopy), with 128 or 256 single-shot EPI images per slice, respectively (TR=2000 ms, TE = 30 ms, TA = 66.6 ms, flip angle = 70°, 64 × 64 matrix, bandwidth=2298 Hz/pixel). The first 8 s of each acquisition were discarded from data analysis in order to achieve a steady state. A total of 166 scans were carried out on the 13 subjects (52 scans to map retinotopy, 26 scans to map MT+, 26 scans to map V6, and 88 scans for the attention experiment). The cortical surface of each subject was reconstructed from a pair of structural scans (T1-weighted MPRAGE, 176 contiguous sagittal slices, 1×1×1 mm; TR=2000 ms, TE = 4.38 ms, flip angle = 8 deg, matrix 256 × 256, bandwidth = 130 Hz/pixel) taken in a separate session. The last scan of each functional session was an alignment scan (also MPRAGE, 1×1×1 mm) acquired in the plane of the functional scans. The alignment scan was used to establish an initial registration of the functional data with the surface. Additional affine transformations that included a small amount of shear were then applied to the functional scans for each subject using blink comparison with the structural images to achieve an exact overlay of the functional data onto each cortical surface.

Data Analysis

Anatomical image processing—FreeSurfer was used for surface reconstruction (Dale et al. 1999; Fischl et al. 1999). The two high resolution structural images obtained from each subject were manually registered and averaged. After reconstructing each hemisphere the inflated occipital lobe was flattened after first cutting it off posterior to the Sylvian fissure and making an additional cut along the calcarine fissure. Stereotaxic coordinates were

calculated through an automatic nonlinear stereotaxic normalization procedure (Friston et al. 1995) performed using the SPM99 software platform (Wellcome Department of Cognitive Neurology, London, UK) and implemented in MATLAB (The MathWorks Inc., Natick, MA, USA). The template image was based on average data provided by the Montreal Neurological Institute (MNI).

Functional image processing—Processing of functional images was performed using FreeSurfer and SPM.

FreeSurfer Analysis—Data from two-condition experiments (i.e., attention experiment, V6 and MT+ mapping) and phase-encoded retinotopy were analyzed by means of a Fourier transform (FT) of the MR time course from each voxel after removing constant and linear terms. This generated a vector with real and imaginary components for each frequency that defined an amplitude and phase of the periodic signal at that frequency. To estimate the significance of the correlation between the blood oxygenation level-dependent (BOLD) signal and the stimulus frequency (8 cycles per scan), the squared amplitude of the signal at the stimulus frequency was divided by the mean of squared amplitudes at all other “noise” frequencies (excluding low-frequency signals due to residual head motion and harmonics of the stimulus frequency). This ratio of two chi-squared statistics follows the F-distribution with degrees of freedom equal to the number of time points and can be used to calculate a significance P-value. Above a minimum threshold, the statistical significance levels of the displayed pseudocolor ranges were normalized according to the overall sensitivity of each subject. These analysis methods were similar to those used in previous studies (Sereno et al. 1995; Tootell et al. 1998; Pitzalis et al., 2006, 2010). The boundaries of retinotopic cortical areas (V1, V2, V3, VP, V3A, V7, V4v and V4/V8) were defined on the cortical surface for each individual subject on the basis of phase-encoded retinotopy (e.g. Sereno et al. 1995) and subsequent calculation of visual field sign. This method provides an objective means of drawing borders between areas based on the angle between the gradients (directions of fastest rate of change) in the polar angle and eccentricity with respect to cortical position (Sereno et al. 1995).

SPM Analysis—In data analyses performed with SPM99, functional images from each participant were co-aligned with the high resolution anatomical scan (MPRAGE) taken in the same session. Images were motion-corrected, transformed into MNI space using a nonlinear stereotaxic normalization procedure (Friston et al. 1995) and smoothed with a three-dimensional Gaussian filter (6 mm full-width-half-maximum). For the block sequence experiments, a general linear model was fit to each individual subject's data, modeling “ON” blocks as box-car functions convolved with a canonical hemodynamic response function. A standard random-effects group analysis was then performed on parameter estimates derived from such general linear models. Significance was judged at the voxel level and by cluster size. Correction for multiple comparisons was performed using distribution approximations from the theory of Gaussian fields at the cluster level ($p \leq 0.01$ corrected), after forming clusters of adjacent voxels surviving a threshold of $p \leq 0.01$ uncorrected. Localization and visualization of individual activations by SPM were achieved by using BrainShow, an in-house software package (code by G. Galati) for visualization of fMRI data. This Matlab-based Analyze-SPM image viewer allows superimposition of individual SPM maps on individual brain slices or on folded, inflated, and flattened representations of cortical surfaces reconstructed by FreeSurfer. This viewer was also used to superimpose SPM group maps (in MNI space, see above) on the cortical surface of the single-subject MNI canonical brain (Colin27) after reconstruction of its cortical surface using FreeSurfer.

Results

Behavioral performance

During the EEG recording the mean hit rate for target detections (79.7%) and reaction time (455 ms) did not differ among stimulus positions ($F_{(3,116)}<1$; n.s.). Nor was there any effect of responding hand. Similarly, during the fMRI scans the mean hit rate for target detections (78.1%) and reaction time (463 ms) did not differ among stimulus positions ($F_{(3,48)}<1$; n.s.). Nor was there any effect of responding hand. No significant differences were found between the EEG and fMRI experiments ($t_{(29)}<1$; n.s.).

ERP Waveforms and Topography

Grand averaged ERPs in response to standard stimuli in each visual quadrant are shown in Figure 2, and the scalp distributions of the major components are mapped in Figures 3 and 4.

At midline occipito-parietal sites the C1 component began at 50-60 ms and peaked at 75-85 ms, showing an inversion in polarity for upper vs. lower visual field. For upper field stimuli this component was negative and largest at occipito-parietal sites slightly ipsilateral to the visual field of the eliciting stimulus. For lower field stimuli the C1 was positive in polarity and was most prominent at occipito-parietal sites slightly contralateral to the visual field of the stimulus. As shown in Table 1, the C1 was not affected by attention. The earliest attention effect was seen as an increased positivity in the second component, a positive deflection peaking around 90-95 ms, hereafter called P1. The P1 attention effect was significant at 90 ms for upper field stimuli and at 95 for lower field stimuli at contralateral sites (P7/P8). The topography of the P1 attention effect for upper quadrants was strongly contralateral at occipito-temporal sites, while for lower quadrants the attention effect was maximal at occipital sites slightly contralateral to the midline (PO3/PO4). The subsequent C2 component at 125-135 ms, like the earlier C1, showed an inversion of polarity for upper vs. lower visual field stimuli. This component was affected by attention and had a maximal voltage over occipito-parietal sites, with a distribution similar to that of the earlier C1 but with opposite polarity.

In the interval between 140 and 180 ms, several spatially and temporally overlapping negative waves showed attentional modulation. At frontal-central sites the most prominent component was the anterior N1a with a mean latency of 145 ms for lower quadrants and 135 ms for upper quadrants, with maximal amplitudes at central sites slightly contralateral to the midline (FC3/FC4). A second negative deflection, N1b, had a mean latency 165 ms and a broad contralateral occipito-parietal focus. A third negative component, N1c, with a mean latency 180 ms for upper field stimuli and 185 ms for lower field stimuli, had a contralateral occipito-temporal distribution with maximal amplitudes located inferiorly (upper field) and laterally (lower field) with respect to the N1b. All these negative components in the N1 family were affected by attention. A substantial attention effect was also found on the subsequent P2 component (mean latency 220 ms for both upper and lower field stimuli), which was largest at central sites (C1/C2) slightly contralateral to the midline. The peak latencies of all these components were not significantly affected by attention (see Table 1). However, it is worth noting that almost all of the attended latencies were shorter than the unattended by 1 to 6 ms, as was found in previous steady-state VEP studies (Di Russo et al. 1999a,b and 2001).

Group fMRI Activations

In the group-averaged data, attention-related fMRI activations were observed in multiple visual cortical areas of the contralateral hemisphere. These included regions of the calcarine fissure, inferior and middle temporal sulci (ITS and MTS respectively), the inferior occipital

cortex (fusiform gyrus and collateral sulcus) and the middle occipital gyrus in and around the posterior intraparietal sulcus (pIPS). Figures 5 and 6 (right panels) show the contralateral activations produced by attention to the pattern reversal stimuli in each quadrant superimposed on the right and left flattened cortical surfaces of the MNI template (group average across subjects). These two figures also show the group-averaged location of the motion sensitive cortex (MT+; dashed outline boxes) that was functionally mapped by additional scans as described in the Methods. The fundus of the parieto-occipital sulcus (POS) is also indicated by dashed lines in the flat maps to aid the anatomical location of area V6. When the upper visual fields were stimulated the attention-related activations were more prominent in ventral visual-cortical areas (the lower bank of the calcarine fissure and the collateral sulcus/fusiform region), whereas for lower visual field stimulation activations were produced mainly in dorsal cortical areas (including the upper bank of the calcarine fissure), as well as in a small region within the fusiform gyrus).

Attention to both upper and lower field stimuli enhanced the BOLD signal in multiple extrastriate regions. The attention-related activation found in the MTS corresponded closely with the group averaged position of the motion sensitive region MT+ (outline boxes in the figures). A prominent activation was also seen in the posterior limb of the IPS (pIPS), which enters the occipital lobe and reportedly extends up to visual areas V3A and V7 (Tootell et al., 1998). More dorsal parietal activations were found on the horizontal segment of the IPS (hIPS, just beyond the extreme medial tip of the IPS), and on the medial POS. The hIPS and the POS have been considered the anatomical landmarks of the LIP area (see Sereno et al., 2001) and V6 area (Pitzalis et al., 2006), respectively. Table 2 gives the MNI coordinates of the centroids of these attention-related activations.

Activations produced by the spatial attention task were greatest in the hemisphere contralateral to the attended visual field. There were no regions with a stronger ipsilateral activation in the present task. It is likely that small ipsilateral fMRI activations were also present, but in the present analysis, which contrasted attend-left and attend-right conditions, any weak ipsilateral mirror foci would not be seen because the spatially coincident contralateral activations produced during attention to the opposite field were larger (for more detail see Di Russo et al 2003).

ERP/fMRI Combination

The first step was to construct a multi-source model of the ERP modulations produced by attention using the BESA algorithm (unseeded model). Dipoles were optimally fit to the attended minus unattended difference waveforms in the time range 70-250 ms (see Methods). Separate source models were calculated for each of the four quadrants. Following the analysis by Di Russo and colleagues (2005), the coordinates of the unseeded dipolar sources (Table 3) were then compared to the locations of the centroids of the attention-related fMRI activations (Table 2). A seeded model was then constructed by moving each dipole's location to that of the nearest fMRI activation and re-fitting the dipole's orientation.

The dipolar sources were fit to the ERP topographies sequentially in the following order: First, a source was fit over 70-120 ms and obtained its best fit closest to area MT+ (RV=3.6% for unseeded model, 3.4% for seeded model, averaged over all quadrants; mean separation between seeded and unseeded dipoles=5.0 mm). The time course of this source accounted for the P1 component attention effect peaking at 95 ms. Second, a source was fit over 100-140 ms and obtained its best fit close to the calcarine fissure (RV=2.2% unseeded, 1.9% seeded; separation=4.3 mm). The time course of this source accounted for the attention effect on the C2 component that peaked at 125-135 ms. Third, a dipole was fit over 135-155 ms and obtained the best fit close to the parietal fMRI activation near the hIPS (RV=3.7% unseeded, 3.5% seeded; separation=13.8 mm). The time course of this source accounted for

the attentional modulation of the N1a component peaking at around 145-150 ms. Fourth, a source was optimized in the 150-170 ms window and obtained its best fit close to the fusiform gyrus activation (RV=3.1% unseeded, 2.9% seeded; separation=5.1 mm). The time course of this source accounted for the N1b attention effect that peaked at around 165 ms. Fifth, a dipole was fit over 160-190 ms and obtained its best fit near the pIPS activation (RV=3.2% unseeded, 3.1% seeded; separation=9.3mm). The time course of this source accounted for the N1c attention effect that peaked at around 180 ms. Finally, to account for the attention effect on the P2 component a source was fit in the 200-250 ms window and obtained its best fit near the POS activation with a peak at around 220-230 ms (RV=3.9% unseeded, 3.8% seeded; separation=7.3mm). The flattened cortical surfaces showed in Figures 5 and 6 show the locations of the best-fit dipolar sources (colored circles) of the preliminary unseeded model for stimuli in each quadrant together with the attention-related fMRI activations. A schematic diagram of the final seeded model for the upper left quadrant is shown as an example in the inset of Figure 5. It should be noted that the N1b source orientation, indicated by light-violet vector, points dorsally while the N1c source orientation, indicated by red vector, points horizontally. This source geometry explains why the N1b topographical distribution (see Figures 3 and 4) is more dorsal than the N1c distribution.

The left panels of Figures 5 and 6 show the source waveforms (time course of dipole moments) in the fMRI seeded locations for stimuli in each of the four quadrants. To show the time course of the attention effect on each source the attended and unattended ERPs were projected into the model that was obtained by fitting the attend minus unattend difference waves as described above. The earliest attention effect can be seen as an increased positivity in the source waveforms of the MT+ source starting at around 70 ms and peaking at 95 ms as the P1 component. This source showed a second modulation with attention (an increased negativity) at around 160 ms. The source waveform of the calcarine dipole showed no evidence of attentional modulation in the latency range of the C1 component (60-100 ms). However, starting at around 100 ms an increase in amplitude in the attended source waveform could be observed that lasted until 150 ms. This attention effect showed a polarity inversion between upper vs. lower field stimuli, and its timing corresponded to the C2 component. The source that was seeded to the parietal hIPS accounted for the amplitude modulation of the N1a component over the time range 135-155 ms and was modulated again at around 210-220 ms. The source seeded to the fusiform gyrus showed attentional modulation over the interval 140-180 ms corresponding to the N1b component (which also received a contribution from the second modulation of the MT+ source) and again at around 200-220 ms. Still later, the source waveform of the dipole seeded to the posterior IPS location showed increased amplitude with attention over the 150-200 ms range that corresponded to the N1c component. Finally, the source localized to the POS showed attention-related activity peaking around 200-250 ms that corresponded with the P2 component. Given that the sources accounting for the N1a and N1b also showed positive modulations at around 200-220 ms, however, and given the widespread distribution of the P2 component on the scalp, it is likely that multiple sources contribute to the P2.

This multi-source model accounted for more than 96.8% of the variance in the scalp topography of the attend minus unattended difference wave for each quadrant over the time range 70-250 ms. The preliminary unseeded models accounted for a maximum of 95.2% of the variance in the same time range. This finding that the seeded dipoles only accounted for a little more variance than the unseeded dipoles suggests that the unseeded model had accurately identified the sources of the attentional modulations that corresponded well with the sites of fMRI activation.

Single Subjects fMRI Activations

Attention-related fMRI activations were localized in each subject with respect to the retinotopically organized visual areas defined on the basis of their calculated field sign and to motion areas MT+ and V6 as defined by functional localizers (see Methods). The borders of retinotopically organized visual areas (V1, V2, V3, VP, V3A, V4v, V7 and V4/V8) and areas V6 and MT+ could be identified for each participant, and activations in striate and adjacent extrastriate visual areas could be distinguished despite their close proximity and individual differences in cortical anatomy.

In individual data, attention to pattern reversal stimulation activated dorsal and ventral visual areas in accordance with their retinotopic representation of lower and upper portions of the visual field. As shown in Figure 7 for a typical subject, when subjects were attending to upper quadrant stimuli, functional responses were found in the lower banks of areas V1 and V2 as well as in areas VP, V4v, V3A+, and V7. This pattern of activations was consistently observed in the majority of subjects: V1+ (64%), V2+ (69%), VP (85%), V4v (81%), V3A+ (89%) and V7 (55%). Attention to upper quadrant stimuli also produced activations in motion sensitive areas MT+ (52%) and V6 (33%), as well as in the lateral occipital region (LOR; 27%) and the horizontal segment of the IPS (hIPS; 37%). The activation observed in the motion sensitive area V6 was in accordance with its retinotopic representation of the upper visual field, which occupies the more medial part of the area (Pitzalis et al., 2006).

When subjects attended to lower quadrant stimuli, activations were consistently produced in the upper banks of V1 (62%) and V2 (92%), and in areas V3 (92%) and V3A (73%). Attention to lower quadrant stimuli also produced activations in motion sensitive areas MT+ (55%), in the LOR (31%) and in the hIPS (33%). Some activation was also found in the retinotopic motion area V6 (15%), specifically in its more lateral part, superior to V3/V3A, where the representation of the lower visual field is located (Pitzalis et al., 2006).

For both upper (73%) and lower (58%) quadrant stimuli, additional attention-related activations were observed in a ventral visual area just anterior to the horizontal meridian representation that marks the anterior border of area V4v (Sereno et al., 1995). Anatomically, this area was located within the collateral sulcus and extended onto the fusiform gyrus. This ventral area most likely corresponds to the color-sensitive area that has been called either V4 (e.g. Zeki and Bartels, 1999) or V8 (Hadjikhani et al., 1998). To avoid controversy, this area will herein be designated V4/V8. Like dorsal V3A, this ventral area represents the entire contralateral hemifield, with superior and inferior portions (on the flat map) representing the lower (-) and upper (+) visual fields, respectively (Hadjikhani et al., 1998; see also Di Russo et al., 2002b, 2003, 2005). Activation of a region corresponding to this ventral visual area was also evident in the group data shown in Figures 5 and 6.

Based on single-subject mappings like those shown in Figure 7, the group-averaged fMRI activations produced by attention to the pattern reversal stimulation may be assigned to specific visual areas. The activations in the calcarine region (proposed source of the C1 and C2 components) appear to originate primarily from area V1, although contributions from the adjoining areas V2 and V3 cannot be excluded. The mid-temporal activations may be assigned to the motion-sensitive area MT+ (proposed source of the P1). The group activations in the fusiform gyrus and collateral sulcus appear to correspond to ventral areas V4v and the color-sensitive area V4/V8 (proposed sources of the N1b). The mid-occipital activations within the pIPS in the group data correspond to activity in dorsal area V3A (proposed source of the N1c). Finally, the parietal activations appear to originate primarily from the hIPS (proposed source of the N1a) and from area V6 within the POS (proposed source of the P2). See Table 2 for coordinates of the centers of these clusters of activation.

Discussion

The present study examined the effects of spatial attention on the cortical processing of a pattern-reversal stimulus. In separate sessions of ERP recording and fMRI subjects attended to a rapid sequence of pattern reversals in one visual field while ignoring a sequence of physically identical reversals in the opposite field. Attention-related ERP modulations and fMRI activations were analyzed jointly in seeded-dipole models to reveal the spatio-temporal patterning of stimulus selection processes in different regions of the visual cortex. It was found that attention did not modulate the amplitude of the earliest component of the ERP (the C1, with an onset latency of 50-60 ms), which was localized to a medial occipital source in or near primary visual cortex (area V1). Over the time range 80-250 ms six different ERP components were identified that showed increased amplitudes for stimuli at attended locations. Five of these components were localized to neural generators in extrastriate visual cortex in temporal (P1), ventral occipital (N1b), dorsal occipital (N1c), superior parietal (N1a) and parieto-occipital (P2) regions. Attention also modulated a longer latency component (C2) that was localized to the same medial occipital area as the C1. We conclude that spatial attention produces a general amplification of sensory signal strength throughout both dorsal and ventral visual pathways and that both feed-forward and feedback signals are enhanced.

The earliest attention effect was found on the P1 component, which had an onset latency of 70-75 ms and peaked at around 95 ms over the lateral occipital scalp. In agreement with the analysis of Di Russo and colleagues (2005), the P1 was localized to a neural generator within a region of the middle temporal sulcus that corresponded to the motion-sensitive MT + area. The short onset latency of this component is compatible with the view that MT+ receives a direct projection from V1 (McKeefry et al., 1997; Tzelepi et al., 2001; Van Rullen and Thorpe, 2001; Vanni et al., 2004). Attention is known to strongly modulate responses in the motion-sensitive region MT+, not only in macaque (e.g., Treue and Maunsell, 1999), but also in human brain (e.g. Tata et al., 2007). It is not surprising that the motion-sensitive area MT+ is activated by pattern-reversal stimuli, because such reversal produces a clear perception of apparent motion that can be described in terms of motion onset and offset responses (Kubova et al., 1995). Consistent with this idea, we did not find activation of MT+ in our previous studies (Di Russo et al., 2002b; 2003) that used pattern-onset stimuli, which did not elicit a perception of motion. In those previous studies the P1 component could be accounted for by neural generators in dorsal occipital (early phase, 70-100 ms) and ventral occipital (late phase, 100-130 ms) regions.

Following the P1, attention produced an amplitude increase in the C2 component peaking at 125-135 ms with a medial occipital distribution very similar to that of the attention-invariant C1. A dipole in medial occipital cortex close to the fMRI activation in area V1 accounted for the attention effect on this component, which, like the C1, also inverted in polarity for upper vs. lower visual field. The presence of such polarity inversion has often been taken as critical evidence for establishing a neural generator in area V1, because of the cruciform organization of the upper and lower banks of the calcarine fissure (e.g. Clark et al. 1995; Di Russo et al. 2005). A recent modeling study (Ales et al., 2010), however, found that neural generators in adjacent areas V2 and V3 may also show polarity inversions on the scalp for upper vs. lower field stimuli for some individuals. In light of this new evidence, we would not rule out contributions of visual areas V2 and V3 to the C1 and C2 components, although our fMRI evidence indicates much larger and more consistent activations in V1 than in V2 or V3. The attentional modulation of C2 observed here strongly resembles the late attention effects beginning around 120-150 ms after stimulus onset that were observed in studies of spatial attention using pattern onset stimuli (Martinez et al. 2001; Noesselt et al. 2002; Di Russo et al. 2003). Those late attention effects also were localized in or near area V1 and

appear to represent attentional enhancement of feedback projections to early visual areas. Such feedback from higher visual areas has been proposed as an essential mechanism of visual perception that may enhance the salience of stimuli at attended locations (e.g., Lamme & Spekreijse 2000; Fahrenfort, Scholte, & Lamme 2008).

Spatial attention strongly modulated several negative components in the "N1 complex" elicited in the interval 140-200 ms, in agreement with previous findings (e.g., Luck et al. 1994; Mangun et al. 2001; Di Russo et al. 2003). The N1 complex consists of at least three negative components that arise from different cortical generators. The N1a (peaking at 145-155 ms) was modeled by a dipolar source in the superior parietal cortex in the vicinity of the horizontal segment of the intraparietal sulcus (hIPS, the most dorsal part of the IPS). The parietal region around the hIPS is generally considered to belong to control networks for spatial attention (e.g. Hopfinger et al. 2000), and its functioning is impaired in neglect patients (Di Russo et al., 2008). This region also corresponds to the parietal area proposed by Sereno et al. (2001) as a putative human homologue of area LIP, which contains a retinotopic mapping of attended locations in contralateral space. The present results suggest that visual input into this parietal region from attended sources is enhanced by spatial attention, in accordance with previous findings (Di Russo et. al., 2003).

Attentional modulation of the N1b component (peaking at 160-165 ms) could be accounted for by dipolar sources in ventral occipital cortex including the fusiform gyrus and collateral sulcus. Attention-related fMRI activations in these areas (VP, V4v, V4/V8) were found to be retinotopically organized, in agreement with previous reports (Sereno et al., 1995; Hadjikhani et al., 1998). While areas VP and V4v were activated by attending to upper visual field stimuli, area V4/V8 was activated by both upper and lower field stimuli. These retinotopic mappings may account for differences in scalp topography of the attention-related amplitude increase of the N1b, which was distributed more ventrally and posteriorly for lower field than upper field stimuli.

The attention-related amplitude increase of the N1c component (180-190 ms) could be accounted for by a dipolar source in the region of the posterior intraparietal sulcus (pIPS). Single subject mapping placed this source in or near area V3A for both upper and lower field stimuli, in accordance with its retinotopic organization (Tootell et al., 1998). The human V3A is a motion sensitive area that is activated by coherent motion, as demonstrated in many previous fMRI studies (e.g. Pitzalis et al., 2010). V3A also has been reported to show activation during spatial attention (e.g., Tootell et al., 1998; Sereno et al., 2001), perhaps as a consequence of its connections with the dorsal ("where") magnocellular stream (reviewed in Felleman and Van Essen, 1991).

Lastly, the attentional modulation of the P2 component at 200-250 ms could be accounted for, at least in part, by a source near the parieto-occipital sulcus (POS) that corresponded to the recently described visual area V6 (Pitzalis et al., 2006). In humans, there have been to our knowledge no previous attempts to detect ERP correlates of V6 activity. Recent work by Pitzalis et al. (2010) has shown that, as in primates, human V6 is a motion-sensitive area, responding much more strongly to coherent than incoherent motion. The present results show in addition that area V6 responds to pattern-reversal stimulation. Neural activity in area V6 appears to be modulated by attention although to a lesser extent than the lateral motion area MT+. One possible explanation is that area V6 in both humans and macaques contains an over-representation of the periphery of the visual field at the expense of the central visual field (e.g. Pitzalis et al, 2006). Activation of POS in the fMRI experiment was less consistent here than in previous studies, probably because the present stimuli were too small (3° in diameter) and eccentric (4° from fixation) to produce robust hemodynamic effects. As noted previously, given that multiple sources are concurrently active in the time

range of the P2 component, it is likely that generators other than the POS contribute to this surface positivity.

The absence of attentional modulation of the C1 component is consistent with a number of previous findings (Clark and Hillyard 1996; Martinez et al. 2001; Noesselt et al. 2002; Woldorff et al. 2002; Di Russo et al. 2003; Fu et al. 2005; Hopfinger & West 2006). Some recent studies have reported that spatial attention can increase the amplitude of the C1 (Kelly et al. 2008; Fu et al. 2009, 2010), but it may be questioned whether these findings actually represent modulation of the initial feed-forward response in area V1. In the experiment of Kelly and colleagues (2008) the left and right field stimuli were always aligned along a diagonal, so that the well-known upper versus lower field polarity inversion seen for the C1 was confounded with a left versus right field inversion, which could have been produced by a laterally oriented dipole outside of area V1. Moreover, the neural sources that were calculated for the attention-related increase in C1 amplitude (using the LAURA algorithm) were situated 23-24 mm lateral to the midline, at the extreme lateral edge of calcarine cortex. Fu and colleagues (2009, 2010) also reported attention related modulation within the C1 latency range (60-90 ms), but this effect appeared to be localized to lateral extrastriate cortex and might have been the result of a sensory interaction between the cue and target stimuli rather than a true attention effect. A recent MEG study (Poghosyan & Ioanides 2008) reported that spatial attention enhanced an early visual response at 55-90 ms that was localized to area V1, but this localization was based on averages of only 18 presentations of each visual stimulus type in each visual field per subject. At present, the evidence that attention can influence the initial evoked response in area V1 appears slim indeed.

The ERP components and sources obtained in the present attention study were very similar to those observed in a prior study (Di Russo et al. 2005), where similar pattern reversal stimuli were presented to subjects who passively viewed them. Moreover, in the present study the waveforms and scalp distributions of the increments of component amplitudes produced by attention were generally very similar to those of the same components when elicited by unattended stimuli. These findings support the view that spatial attention operates primarily by increasing the gain of sensory-evoked neural responses (Posner and Dehaene, 1994; Hillyard et al., 1998) rather than by recruiting a different population of neurons, and that this gain control or amplification mechanism is operative in many visual-cortical areas. The fMRI activations produced during attention showed a strong retinotopic organization in many cortical areas, which suggests that the cortical mapping of visual field location might provide the neural substrate for spatially directed attention (Yantis, 2008).

Overall, the results described here help to reveal the timing and the neuro-anatomical bases of stimulus selection processes and to characterize the roles of extrastriate and striate cortex in visuo-spatial attention. In agreement with previous studies, no evidence was obtained to suggest that attended stimuli are preferentially processed during the initial feed-forward response in striate cortex (area V1) at 50-80 ms after stimulus onset. However, longer latency activity peaking at 125-135 ms that was localized to early cortical generators in or near area V1 was enhanced by attention. Beginning at about 80 ms after stimulus presentation attended-location stimuli elicited enlarged neural responses in multiple extrastriate visual areas in the occipital, parietal, and temporal lobes. The timing of this neural activity modulated by attention was established by electrophysiological recordings of ERPs, and the localization of the underlying generators was reinforced by the mapping of hemodynamic responses in a parallel fMRI experiment. These findings support the hypothesis that a sensory gain-control mechanism selectively amplifies both feed-forward and feedback responses elicited by attended-location stimuli in multiple visual cortical areas of both the dorsal and ventral streams of processing.

Acknowledgments

This work was supported by grants from the Italian Ministry of Education (MIUR prot. 2007JLKBL9_004) and Santa Lucia Foundation and from the U.S. Office of Naval Research (N00014-07-1-0937) and National Institute of Mental Health (MH-86385).

References

1. Aine CJ, Supek S, George JS, Ranken D, Lewine J, Sanders J, Best E, Tiee W, Flynn ER, Wood CC. Retinotopic organization of human visual cortex: departures from the classical model. Cereb Cortex. 1996; 6:354–361. [PubMed: 8670663]
2. Ales JM, Yates JL, Norcia AM. V1 is not uniquely identified by polarity reversals of responses to upper and lower visual field stimuli. Neuroimage. 2010; 52:1401–1409. [PubMed: 20488247]
3. Clark VP, Fan S, Hillyard SA. Identification of early visually evoked potential generators by retinotopic and topographic analysis. Hum Brain Mapp. 1995; 2:170–187.
4. Clark V, Hillyard SA. Spatial selective attention affects early extrastriate but not striate components of the visual evoked potential. J Cog Neurosci. 1996; 8:387–402.
5. Dale AM, Halgren E. Spatiotemporal mapping of brain activity by integration of multiple imaging modalities. Curr Opin Neurobiol. 2001; 11:202–208. [PubMed: 11301240]
6. Dale AM, Fischl Bruce, Sereno MI. Cortical Surface-Based Analysis I: Segmentation and Surface Reconstruction. Neuroimage. 1999; 9:179–194. [PubMed: 9931268]
7. Di Russo F, Spinelli D. Electrophysiological evidence for an early attentional mechanism in visual processing in humans. Vis Res. 1999a; 39:2975–2985. [PubMed: 10664797]
8. Di Russo F, Spinelli D. Spatial attention has different effects on the magno- and parvo-cellular pathways. NeuroReport. 1999b; 10:2755–2762. [PubMed: 10511435]
9. Di Russo F, Spinelli D, Morrone MC. Automatic gain control contrast mechanisms are modulated by attention in humans: evidence from visual evoked potentials. Vis Res. 2001; 41:2335–2347.
10. Di Russo F, Spinelli D. Effects of sustained, voluntary attention on amplitude and latency of steady-state visual evoked potential: a costs and benefits analysis. Clin Neurophysiol. 2002a; 113:1771–1777. [PubMed: 12417230]
11. Di Russo F, Martínez A, Sereno MI, Pitzalis S, Hillyard SA. The cortical sources of the early components of the visual evoked potential. Hum Brain Mapp. 2002b; 15:95–111. [PubMed: 11835601]
12. Di Russo, F.; Teder-Sälejärvi, WA.; Hillyard, SA. Steady-State VEP and attentional visual processing. In: Zani, A.; Proverbio, AM., editors. The cognitive electrophysiology of mind and brain. Academic Press; 2002c. p. 259-274.
13. Di Russo F, Martínez A, Hillyard SA. Source analysis of event-related cortical activity during visuo-spatial attention. Cereb Cortex. 2003; 13:486–499. [PubMed: 12679295]
14. Di Russo F, Pitzalis S, Spitoni G, Aprile T, Patria F, Spinelli D, Hillyard SA. Identification of the neural sources of the pattern-reversal VEP. Neuroimage. 2005; 24:874–886. [PubMed: 15652322]
15. Di Russo F, Pitzalis S, Aprile T, Spitoni G, Patria F, Stella A, Spinelli D, Hillyard SA. Spatio-Temporal Analysis of the Cortical Sources of the Steady-State Visual Evoked Potential. Hum Brain Mapp. 2007; 28:323–334. [PubMed: 16779799]
16. Di Russo F, Aprile T, Spitoni G, Spinelli D. Impaired Visual Processing of Contralesional Stimuli in Neglect Patients: A Visual-Evoked Potential Study. Brain. 2008; 131:842–854. [PubMed: 18024488]
17. Fahrenfort JJ, Scholte HS, Lamme VA. The spatiotemporal profile of cortical processing leading up to visual perception. J Vis. 2008; 8:1–12. [PubMed: 18318615]
18. Fattori P, Pitzalis S, Galletti C. The cortical visual area V6 in macaque and human brains. J Physiol -Paris. 2009; 103:88–97. [PubMed: 19523515]
19. Felleman DJ, Van Essen DC. Distributed hierarchical processing in the primate cerebral cortex. Cereb Cortex. 1991; 1:1–47. [PubMed: 1822724]
20. Fischl B, Sereno MI, Dale AM. Cortical Surface-Based Analysis II: Inflation, Flattening, and a Surface-Based Coordinate System. Neuroimage. 1999; 9:195–207. [PubMed: 9931269]

21. Friston KJ, Frith CD, Turner R, Frackowiak RS. Characterizing evoked hemodynamics with fMRI. Neuroimage. 1995; 2:157–165. [PubMed: 9343598]
22. Fu S, Fedota JR, Greenwood PM, Parasuraman R. Dissociation of visual C1 and P1 components as a function of attentional load: an event-related potential study. Biol Psychol. 2010; 85:171–178. [PubMed: 20599467]
23. Fu S, Greenwood PM, Parasuraman R. Brain mechanisms of involuntary visuospatial attention: an event-related potential study. Hum Brain Mapp. 2005; 25:378–390. [PubMed: 15852465]
24. Fu S, Huang Y, Luo Y, Wang Y, Fedota J, Greenwood PM, Parasuraman R. Perceptual load interacts with involuntary attention at early processing stages: event-related potential studies. Neuroimage. 2009; 48:191–199. [PubMed: 19539769]
25. Hadjikhani N, Liu AK, Dale AM, Cavanagh P, Tootell RB. Retinotopy and color sensitivity in human visual cortical area V8. Nat Neurosci. 1998; 1:235–241. [PubMed: 10195149]
26. Halliday, AM. Evoked Potentials in Clinical Testing. 2nd. Edinburgh: Churchill Livingstone; 1993.
27. Hashimoto T, Kashii S, Kikuchi M, Honda Y, Nagamine T, Shibasaki H. Temporal profile of visual evoked responses to pattern reversal stimulation analyzed with a whole-head magnetometer. Exp Brain Res. 1999; 125:375–382. [PubMed: 10229028]
28. Hillyard SA, Anllo-Vento L. Event-related brain potentials in the study of visual selective attention. Proc Natl Acad Sci USA. 1998; 95:781–787. [PubMed: 9448241]
29. Hillyard SA, Vogel EK, Luck SJ. Sensory gain control (amplification) as a mechanism of selective attention: electrophysiological and neuroimaging evidence. Philos Trans R Soc Lond B Biol Sci. 1998; 353:1257–1267. [PubMed: 9770220]
30. Hopf, JM.; Heinze, HJ.; Schoenfeld, MA.; Hillyard, SA. Spatio-temporal analysis of visual attention. In: Gazzaniga, MS., editor. The Cognitive Neurosciences IV. Cambridge, MA: MIT Press; 2009. p. 235-250.
31. Hopfinger JB, Buonocore MH, Mangun GR. The neural mechanisms of top-down attentional control. Nat Neurosci. 2000; 3:284–291. [PubMed: 10700262]
32. Hopfinger, JB.; Luck, SJ.; Hillyard, SA. Selective attention: Electrophysiological and neuromagnetic studies. In: Gazzaniga, MS., editor. The Cognitive Neurosciences III. Cambridge, MA: MIT Press; 2004. p. 561-574.
33. Hopfinger JB, West VM. Interactions between endogenous and exogenous attention on cortical visual processing. Neuroimage. 2006; 31:774–789. [PubMed: 16490366]
34. Kelly SP, Gomez-Ramirez M, Foxe JJ. Spatial attention modulates initial afferent activity in human primary visual cortex. Cereb Cortex. 2008; 18:2629–2636. [PubMed: 18321874]
35. Kubova Z, Kuba M, Spekreijse H, Blakemore C. Contrast dependence of motion-onset and pattern-reversal evoked potentials. Vision Res. 1995; 35:197–205. [PubMed: 7839616]
36. Lamme, VAF.; Spekreijse, H. Contextual modulation in primary visual cortex and scene perception. In: Gazzaniga, MS., editor. The new Cognitive Neurosciences. Cambridge, MA: MIT Press; 2000. p. 279-290.
37. Luck SJ, Hillyard SA, Mouloua M, Woldorff MG, Clark VP, Hawkins HL. Effect of spatial cuing on luminance detectability: Psychophysical and electrophysiological evidence for early selection. J Exp Psychol: Hum percep perform. 1994; 20:1000–1014.
38. Mangun GR, Hinrichs H, Scholz M, Mueller-Gaertner HW, Herzog H, Krause BJ, Tellman L, Kemna L, Heinze HJ. Integrating electrophysiology and neuroimaging of spatial selective attention to simple isolated visual stimuli. Vis Res. 2001; 41:1423–1435. [PubMed: 11322984]
39. Martinez A, Di Russo F, Anllo-Vento L, Sereno MI, Buxton RB, Hillyard SA. Putting spatial attention on the map: timing and localization of stimulus selection processes in striate and extrastriate visual areas. Vision Res. 2001; 41:1437–1457. [PubMed: 11322985]
40. McKeefry DJ, Zeki S. The position and topography of the human colour centre as revealed by functional magnetic resonance imaging. Brain. 1997; 120:2229–2242. [PubMed: 9448578]
41. Müller MM, Teder-Salejarvi W, Hillyard SA. The time course of cortical facilitation during cued shifts of spatial attention. Nat Neurosci. 1998b; 1:631–634.
42. Müller MM, Malinowski P, Gruber T, Hillyard SA. Sustained division of the attentional spotlight. Nature. 2003; 424:309–12. [PubMed: 12867981]

43. Murray MM, Wylie GR, Higgins BA, Javitt DC, Schroeder CE, Foxe JJ. The spatiotemporal dynamics of illusory contour processing: combined high-density electrical mapping, source analysis, and functional magnetic resonance imaging. J Neurosci. 2002; 22:5055–5073. [PubMed: 12077201]
44. Nakamura A, Kakigi R, Hoshiyama M, Koyama S, Kitamura Y, Shimojo M. Visual evoked cortical magnetic fields to pattern reversal stimulation. Brain Res Cogn Brain Res. 1997; 6:9–22. [PubMed: 9395846]
45. Noesselt T, Hillyard SA, Woldorff MG, Schoenfeld A, Hagner T, Jäncke L, Tempelmann C, Hinrichs H, Heinze HJ. Delayed striate cortical activation during spatial attention. Neuron. 2002; 35:575–587. [PubMed: 12165478]
46. Pitzalis S, Galletti C, Huang RS, Patria F, Committeri G, Galati G, Fattori P, Sereno MI. Wide-field retinotopy defines human cortical visual area V6. J Neurosci. 2006; 26:7962–7973. [PubMed: 16870741]
47. Pitzalis S, Sereno MI, Committeri G, Fattori P, Galati G, Patria F, Galletti C. Human V6: the medial motion area. Cereb Cortex. 2010; 20:411–424. [PubMed: 19502476]
48. Poghosyan V, Ioannides AA. Attention modulates earliest responses in the primary auditory and visual cortices. Neuron. 2008; 58:802–813. [PubMed: 18549790]
49. Posner MI, Dehaene S. Attentional networks. Trend in Neurosciences. 1994; 17:75–79.
50. Regan, D. Human brain electrophysiology: evoked potentials and evoked magnetic fields in science and medicine. New York: Elsevier; 1989.
51. Schoenfeld MA, Hopf JM, Martinez A, Mai HM, Sattler C, Gasde A, Heinze HJ, Hillyard SA. Spatio-temporal analysis of feature-based attention. Cerebral Cortex. 2007; 10:2468–2477. [PubMed: 17204821]
52. Sereno MI, Dale AM, Reppas JB, Kwong KK, Belliveau JW, Brady TJ, Rosen BR, Tootell RBH. Borders of multiple visual areas in humans revealed by functional magnetic resonance imaging. Science. 1995; 268:889–893. [PubMed: 7754376]
53. Sereno MI, Pitzalis S, Martínez A. Mapping of contralateral space in retinotopic coordinates by a parietal cortical area in humans. Science. 2001; 294:1350–1354. [PubMed: 11701930]
54. Shigeto H, Tobimatsu S, Yamamoto T, Kobayashi T, Kato M. Visual evoked cortical magnetic responses to checkerboard pattern reversal stimulation: A study on the neural generators of N75, P100 and N145. J Neurol Sci. 1998; 156:186–194. [PubMed: 9588856]
55. Tata MS, Mason AL, Sutherland RJ. Attention modulates responses to motion reversals in human visual cortex. Neuroreport. 2007; 18:1361–1365. [PubMed: 17762713]
56. Tootell RBH, Hadjikhani N, Hall EK, Marrett S, Vanduffel W, Vaughan JT, Dale AM. The retinotopy of visual spatial attention. Neuron. 1998; 21:1409–1422. [PubMed: 9883733]
57. Tootell RBH, Taylor JB. Anatomical evidence for MT and additional cortical visual areas in humans. Cereb Cortex. 1995; 5:39–55. [PubMed: 7719129]
58. Treue S, Maunsell JH. Effects of attention on the processing of motion in macaque middle temporal and medial superior temporal visual cortical areas. J Neurosci. 1999; 19:7591–7602. [PubMed: 10460265]
59. Tzelepi A, Ioannides AA, Poghosyan V. Early (N70m) neuromagnetic signal topography and striate and extrastriate generators following pattern onset quadrant stimulation. NeuroImage. 2001; 13:702–718. [PubMed: 11305898]
60. Valdes-Sosa PA, Sanchez-Bornot JM, Sotero RC, Iturria-Medina Y, Aleman-Gomez Y, Bosch-Bayard J, Carbonell F, Ozaki T. Model driven EEG/fMRI fusion of brain oscillations. Hum Brain Mapp. 2009; 30:2701–2721. [PubMed: 19107753]
61. Van Rullen R, Thorpe SJ. The time course of visual processing: from early perception to decision-making. J Cog Neurosci. 2001; 131:454–461.
62. Vanni S, Warnking J, Dojat M, Delon-Martin C, Bullier J, Segebarth C. Sequence of pattern onset responses in the human visual areas: an fMRI constrained VEP source analysis. Neuroimage. 2004; 21:801–817. [PubMed: 15006647]
63. Woldorff MG, Liotti M, Seabolt M, Busse L, Lancaster JL, Fox PT. The temporal dynamics of the effects in occipital cortex of visual-spatial selective attention. Brain Res Cogn Brain Res. 2002; 15:1–15. [PubMed: 12433379]

64. Yantis S. The Neural Basis of Selective Attention: Cortical Sources and Targets of Attentional Modulation. Curr Dir Psychol Sci. 2008; 17:86–90. [PubMed: 19444327]

65. Zeki S, Bartels A. The clinical and functional measurement of cortical (in) activity in the visual brain, with special reference to the two subdivisions (V4 and V4 alpha) of the human colour centre. Philos Trans R Soc Lond B: Biol Sci. 1999; 354:1371–1382. [PubMed: 10466157]

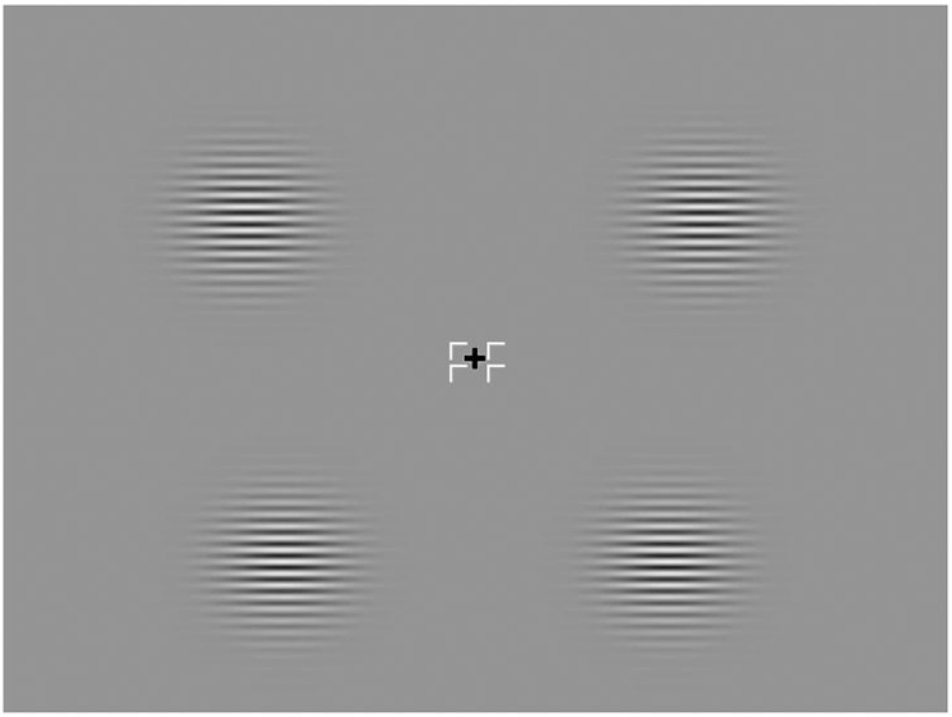

Figure 1.
Standard stimuli used in this experiment. Circular Gabor patches were continuously present in either the upper or lower visual quadrants. At intervals of 350-650 ms either the left or the right patch (in a randomized sequence) underwent phase reversal for 66 ms then returned to the original phase.

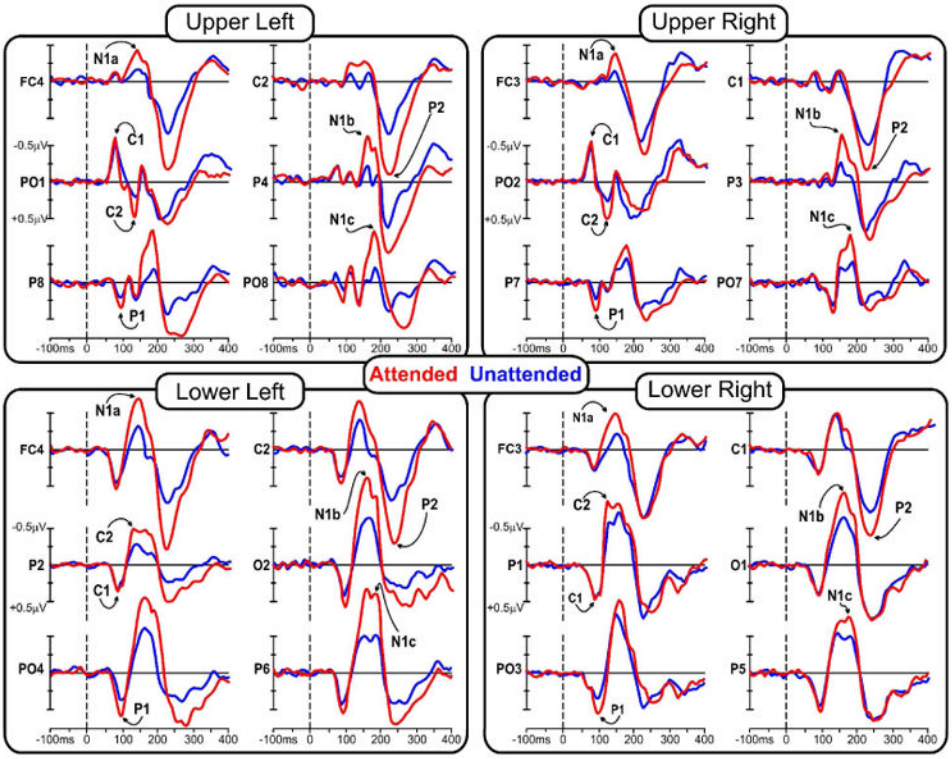

Figure 2.
Grand averaged waveforms of the ERPs to stimuli in each of the quadrants when those stimuli were attended (red line) and unattended (blue line).

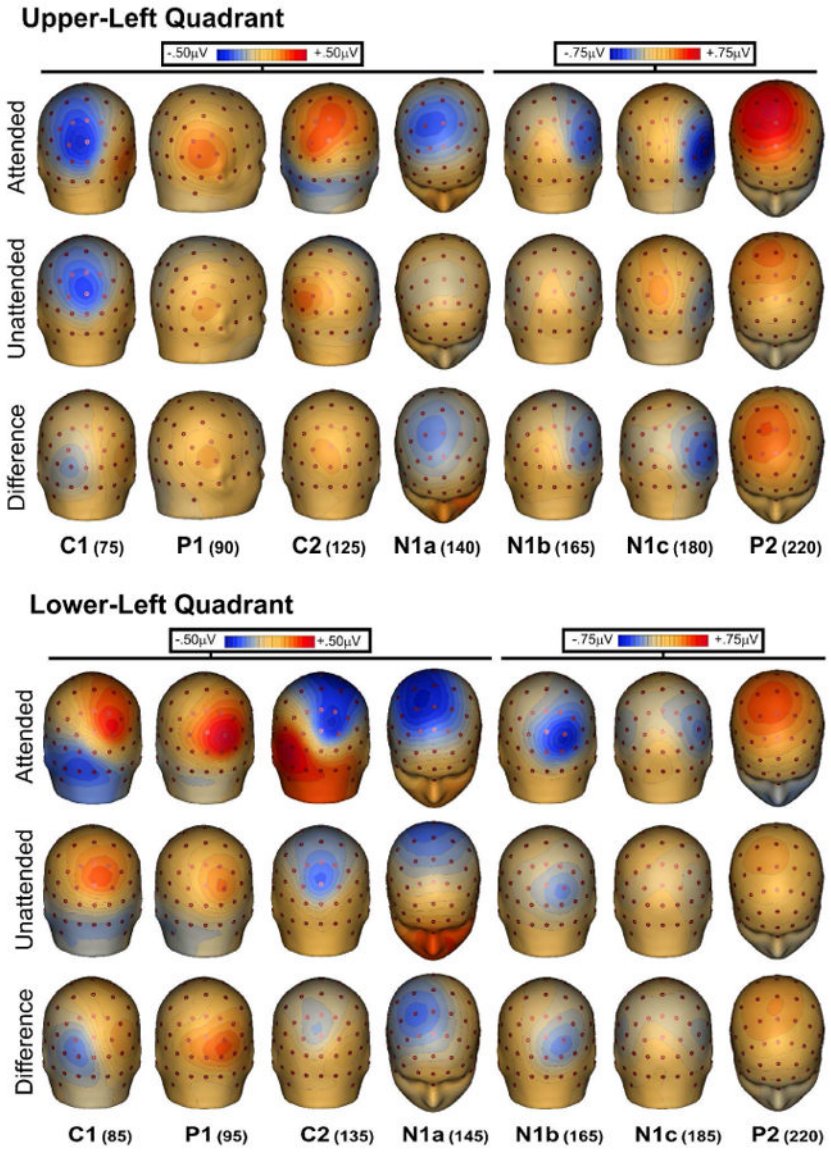

Figure 3.

Spline-interpolated 3D voltage maps of the various components in the grand averaged waveforms for ERPs to stimuli in the left quadrants. Maps of each component are shown at the indicated latencies for attended, unattended, and difference (attended minus unattended) waveforms.

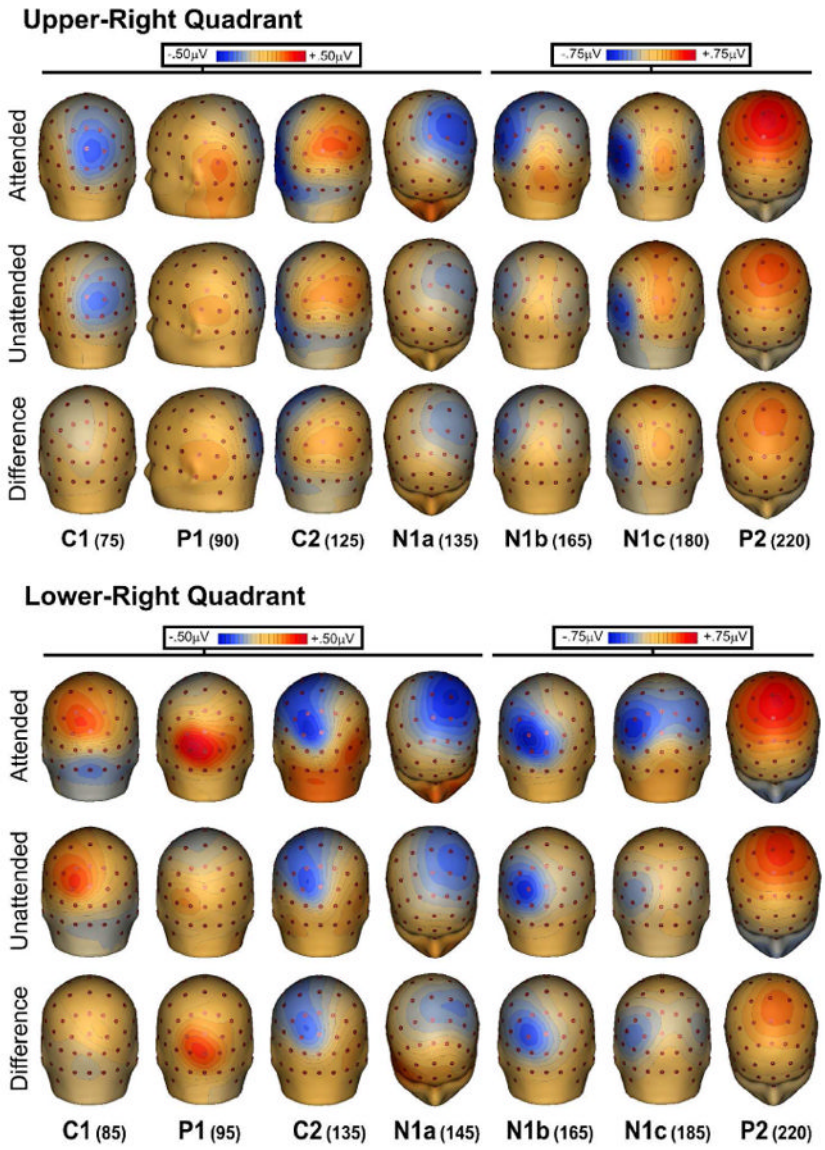

Figure 4.

Spline-interpolated 3D voltage maps of the various components in the grand averaged waveforms for ERPs to stimuli in the right quadrants. Maps of each component are shown at the indicated latencies for attended, unattended, and difference (attended minus unattended) waveforms.

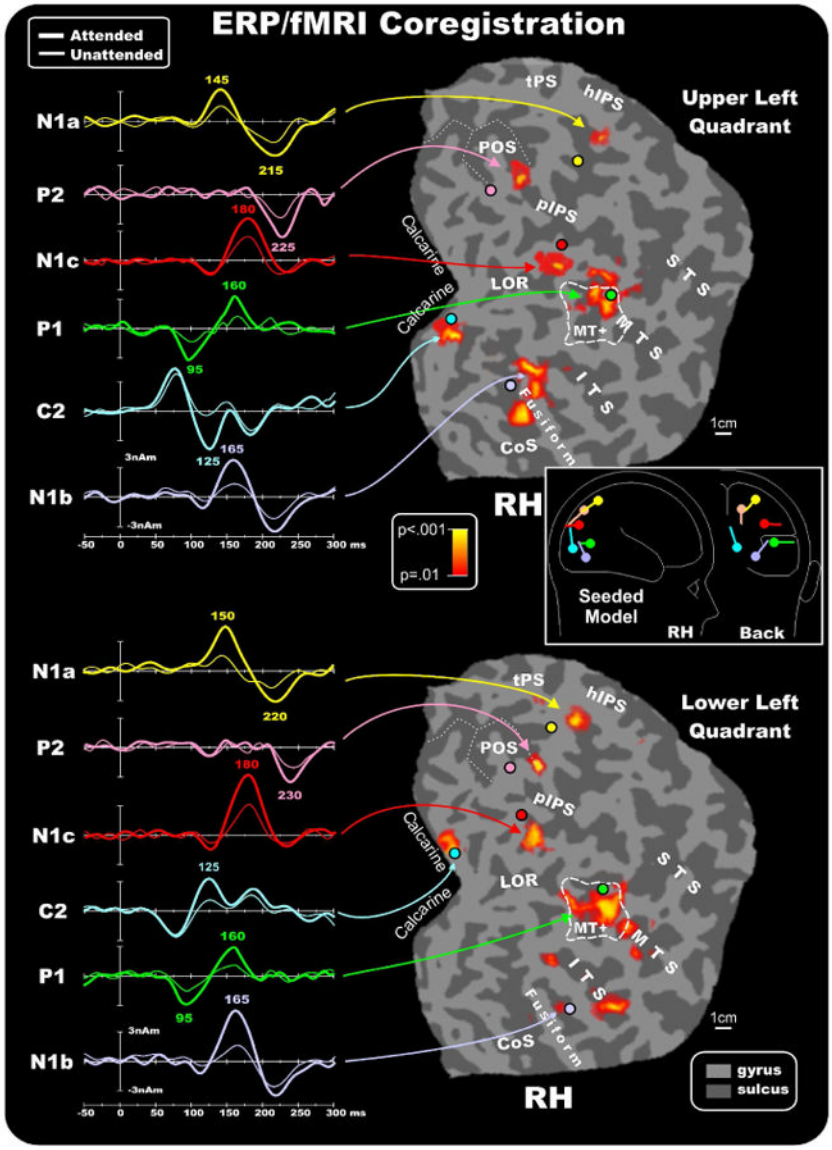

Figure 5.

Combination of the ERP/fMRI attention effects in the right hemisphere for contralateral stimuli in the upper and lower quadrants. The left panels show the source waveforms of the dipoles fit to the grand averaged ERPs and seeded to the fMRI activations indicated by arrows (listed in Table 2). Right panels show group-averaged contralateral fMRI activations superimposed on the flattened hemisphere (occipital lobe) of the MNI template. Circles indicate the locations of the dipoles in the unseeded model listed in Table 3. The pseudocolor scale in the center of the figure indicates the statistical significance of the fMRI activations. Major sulci (dark gray) are labeled as follows: parieto-occipital sulcus (POS), transverse segment of the parietal sulcus (tPS), intraparietal sulcus (IPS), superior temporal sulcus (STS), middle temporal sulcus (MTS), inferior temporal sulcus (ITS), lateral occipital region (LOR), fusiform gyrus (Fusiform) and calcarine fissure (Calcarine). The fundus of the POS is indicated by dashed lines. The dashed outline surrounding MT+ represents the group-averaged location of the motion sensitive cortex based on separate localizer scans. Inset shows as an example the schematic representation of the source locations and

orientations in the seeded dipole model of the upper left quadrant attention effect. Similar models were obtained for the other quadrants.

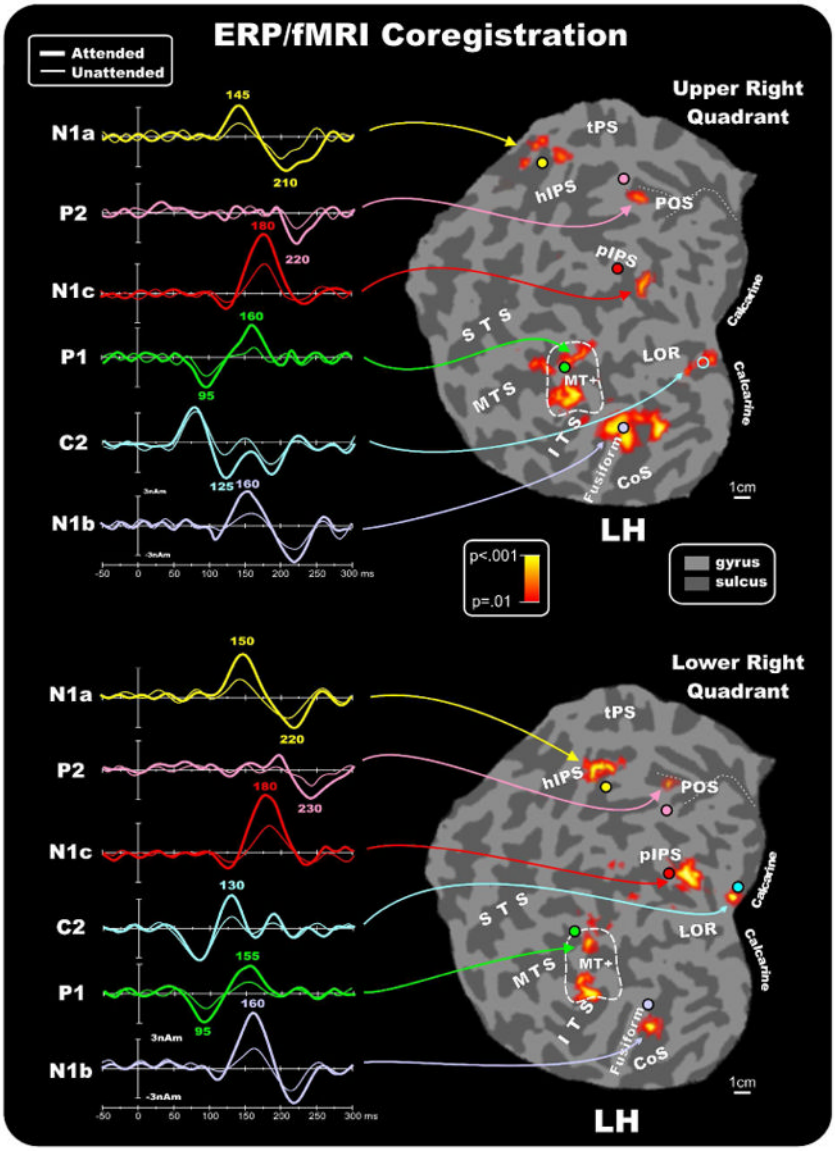

Figure 6.
Same as figure 5 for the attention effects in the left hemisphere for contralateral stimulation.

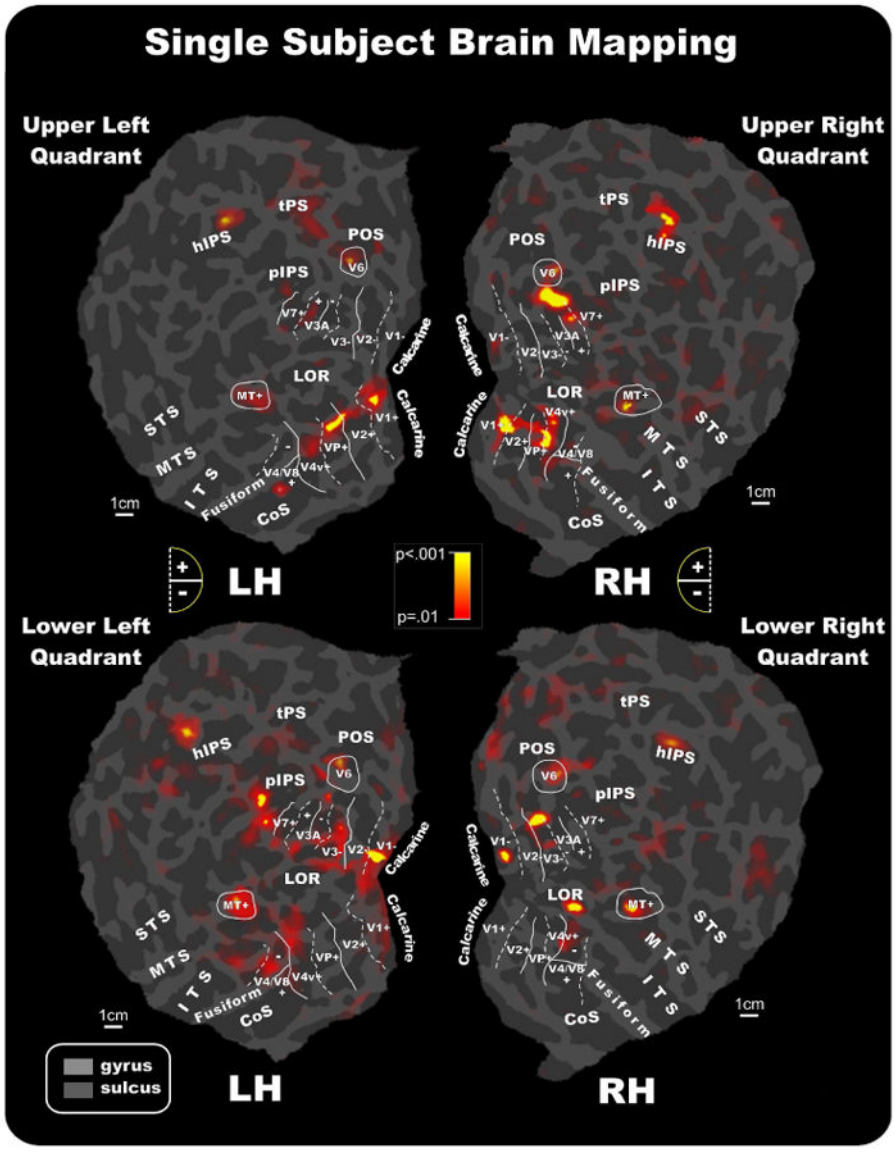

Figure 7.

Attention-related fMRI activations projected onto the flattened left and right hemispheres of an individual participant. Activations in response to contralateral stimuli in each quadrant are shown in relation to the boundaries of visual areas defined in the same subject by the retinotopic visual field sign, and by MT+ and V6 mapping. As indicated in the semicircular logos, dashed and solid lines correspond to vertical and horizontal meridians, respectively; the plus and minus symbols refer to upper and lower visual fields representations, respectively. Other labels and logos are as in Figures 5 and 6.

Table 1

Mean peak latencies (ms), amplitudes (μV) and significance levels of attention effects on ERP components. Peak measurements were made within the latency intervals and at the electrode sites as indicated.

Upper Left Quadrant		Latency			Amplitude		
Component	**Sensor**	**Attended**	**Unattended**	**p**	**Attended**	**Unattended**	**p**
C1 (60-100)	PO1	78	82	ns	-0.68	-0.64	n.s.
P1 (80-110)	P8	94	96	ns	0.39	0.21	<.05
C2 (100-150)	PO1	128	132	ns	0.45	0.22	<.05
N1a (130-160)	FC4	144	146	ns	-0.43	-0.18	<.05
N1b (150-180)	P4	164	166	ns	-0.66	-0.23	<.02
N1c (170-200)	PO8	180	184	ns	-0.74	-0.21	<.01
P2 (200-250)	C2	218	222	ns	1.39	0.71	<.005
Lower Left Quadrant							
C1 (60-100)	P2	84	86	ns	0.38	0.36	n.s.
P1 (80-110)	PO4	96	96	ns	0.65	0.41	<.05
C2 (100-150)	P2	128	130	ns	-0.52	0.27	<.05
N1a (130-160)	FC4	148	148	ns	-0.72	-0.31	<.02
N1b (150-180)	O2	164	166	ns	-1.18	-0.64	< .01
N1c (170-200)	P6	180	182	ns	-1.08	0.49	< .01
P2 (200-250)	C2	229	231	ns	1.26	0.71	<.02
Upper Right Quadrant							
C1 (60-100)	PO2	76	78	ns	-0.59	-0.52	n.s.
P1 (80-110)	P7	95	96	ns	0.38	0.26	<.05
C2 (100-150)	PO2	124	126	ns	0.51	0.25	<.05
N1a (130-160)	FC3	144	146	ns	-0.39	-0.15	<.05
N1b (150-180)	PO7	158	162	ns	-0.75	-0.26	<.02
N1c (170-200)	P3	180	184	ns	-0.66	-0.28	<.05
P2 (200-250)	C1	215	221	ns	1.25	0.81	< .01
Lower Right Quadrant							
C1 (60-100)	P1	86	86	ns	0.5	0.48	n.s.

Upper Left Quadrant		Latency			Amplitude		
Component	**Sensor**	**Attended**	**Unattended**	**p**	**Attended**	**Unattended**	**p**
P1 (80-110)	PO3	96	97	ns	0.63	0.36	<.05
C2 (100-150)	P1	128	130	ns	-0.94	-0.61	<.05
N1a (130-160)	FC3	148	150	ns	-0.52	-0.22	<.05
N1b (150-180)	O1	161	163	ns	-0.98	-0.66	<.02
N1c (170-200)	P5	180	183	ns	-0.77	0.49	<.05
P2 (200-250)	C1	229	232	ns	1.24	0.87	<.01

Table 2

Talairach coordinates of the significant attention-related activations in the average fMRI data over thirteen subjects. Coordinates are given for the centroids of contralateral activations in response to stimuli in each of the four quadrants (values are in mm).

Upper Left	**X**	**Y**	**Z**	**Upper Right**	**X**	**Y**	**Z**
Calcarine	9	-87	-1	Calcarine	-3	-88	-3
Collateral Occipital sulcus	30	-58	-2	Inferior Temporal sulcus	-21	-79	-7
Fusiform gyrus	27	-70	-9	Fusiform gyrus	-24	-73	-9
Middle Temporal sulcus	45	-67	5	Middle Temporal sulcus	-48	-70	7
Posterior Intra-Parietal sulcus	36	-83	24	Posterior Intra-Parietal sulcus	-18	-90	18
Parietal Occipital sulcus	18	-82	43	Parietal Occipital sulcus	-16	-80	40
Horizontal Intra-Parietal sulcus	25	-55	52	Horizontal Intra-Parietal sulcus	-36	-50	58
Lower Left	**X**	**Y**	**Z**	**Lower Right**	**X**	**Y**	**Z**
Calcarine	6	-90	14	Calcarine	-3	-96	10
Fusiform gyrus	30	-53	-10	Fusiform gyrus	-36	-62	-10
Inferior Temporal sulcus	48	-47	-10	Inferior Temporal sulcus	-42	-67	-7
Middle Temporal sulcus	42	-65	5	Middle Temporal sulcus	-48	-78	6
Posterior Intra-Parietal sulcus	12	-80	37	Posterior Intra-Parietal sulcus	-11	-98	16
Parietal Occipital sulcus	20	-81	45	Parietal Occipital sulcus	-20	-76	41
Horizontal Intra-Parietal sulcus	31	-63	52	Horizontal Intra-Parietal sulcus	-30	-55	46

Table 3

Talairach coordinates of the unseeded dipoles in models that were fit to the attended minus unattended grand-average difference waveforms (values are in mm).

Upper Left	**X**	**Y**	**Z**	**Upper Right**	**X**	**Y**	**Z**
P1	42	-64	2	P1	-44	-68	4
C2	6	-90	1	C2	-5	-85	-5
N1a	27	-74	49	N1a	-32	-63	54
N1b	30	-76	-12	N1b	-23	-74	-10
N1c	33	-85	30	N1c	-25	-75	32
P2	14	-79	40	P2	-20	-85	44
Lower Left	**X**	**Y**	**Z**	**Lower Right**	**X**	**Y**	**Z**
P1	44	-62	6	P1	-44	-75	3
C2	7	-88	11	C2	-4	-94	14
N1a	25	-80	48	N1a	-25	-68	47
N1b	32	-56	-11	N1b	-32	-67	-7
N1c	15	-78	39	N1c	-13	-94	15
P2	18	-82	39	P2	-18	-83	35